# Coupling between elastic strains and phase transition in dense pure zirconia polycrystals

René Guinebretière,[1,*] Taylan Ors,[2,3] Vincent Michel,[2] Elsa Thune,[1] Marc Huger,[1] Stephan Arnaud,[4] Nils Blanc,[4] Nathalie Boudet,[4] and Olivier Castelnau[2]

[1]*Université de Limoges, IRCER, UMR CNRS 7315, 12 rue Atlantis, Limoges 87068, France*
[2]*PIMM, UMR CNRS 8006, ENSAM, CNAM, 151 boulevard de l'Hôpital, Paris 75013, France*
[3]*Université de Haute-Alsace, IS2M, CNRS, UMR 7361, 3bis rue Alfred Werner, 68093 Mulhouse Cedex, France*
[4]*Université Grenoble Alpes, CNRS, Institut Néel UPR CNRS 2940, 38000 Grenoble, France*

(Received 16 July 2021; accepted 20 December 2021; published 5 January 2022)

A deep understanding of the solid-state phase transition processes of zirconia is a mandatory requirement for the development of new zirconia-based materials useful for many industrial applications. For five decades, the monoclinic ⇔ tetragonal phase transition is described as a martensitic one and it is well known that it is associated with a large unit cell volume variation that promotes the appearance of elastic strains and also microcracking. In the present paper, we study, through *in situ* high temperature x-ray diffraction experiments, the coupling between strain relaxation and the martensitic phase transition into a pure zirconia bulk polycrystal. Quantitative analysis of the diffraction signal allows us to disentangle, with respect to the temperature variation, the phase transition and the microcracking processes, and we demonstrate that a high temperature postelaboration thermal treatment induces an increase in the stored elastic energy. Finally, we show that in such polycrystals exhibiting a crystal size distribution and in which the crystals are under internal stresses, the tetragonal to monoclinic phase transition process evolves from a first order one to a second order one when the temperature decreases.

DOI: 10.1103/PhysRevMaterials.6.013602

## I. INTRODUCTION

Zirconia is one of the most used oxide compounds. It exhibits high temperature mechanical and ionic transport properties, and a large part of its characteristics is directly related to the ability of zirconium to accommodate different coordinations leading to the crystallization of zirconia under different phases depending on the pressure and the temperature. Under atmospheric pressure, pure zirconia free of stress solidifies into a cubic crystal structure (space group $Fm\bar{3}m$) at about 2700 °C, transforms to tetragonal (space group $P4_2/nmc$) upon cooling to 2300 °C, and becomes monoclinic (space group $P2_1/c$) at 1170 °C [1]. Several other phases have been evidenced under high pressure [2]. The solid-state phase transition (SPT) between the tetragonal and monoclinic phases ($m \Leftrightarrow t$) is a first order one and is of martensitic type [3–5]. It induces a large volume expansion that creates huge internal stresses in the material, which promotes the development of a microcrack network and often the breakage of pure zirconia based dense materials. Nevertheless, it is well known that accurate control of this phase transition, and thus the formation of microcracks, allows the production of materials exhibiting enhanced mechanical properties [6]. Besides temperature and external pressure, the $m \Leftrightarrow t$ SPT can be controlled through mainly two different ways, i.e., the formation of solid solutions introducing aliovalent cations to substitute for zirconium [7–9] and a complex balance between the size of the zirconia crystals and the local stresses [10–14]. The first aspect has been extensively studied in order to promote transformation toughening of ceramics [15,16] as well as to develop ionic conductors [17] used as oxygen sensors or as basic components of solid oxide fuel cells.

The understanding of the relationships between the $m \Leftrightarrow t$ SPT and the crystal size is a more complex scientific topic. Because of the strong volume variation associated with the transition [1], local strains promote stresses that have a strong influence on the transition temperature. Since the pioneering work of Garvie [18], it is well known that a decrease in the crystal size in the nanometers range induces a decrease in the $t \rightarrow m$ transition temperature. It is usually accepted that free pure zirconia particles with a diameter below 30 nm are stable at room temperature under the tetragonal phase. This feature is not fully understood, but it has been studied for nanosized zirconia crystals free of any external constraint [14] or zirconia based high K [19] or ferroelectric [20] very thin films. In most of the cases, free nanosized zirconia particles or zirconia based thin films are elaborated through processes that avoid the use of high temperatures, and very often, zirconia nanosized particles crystallize under the metastable tetragonal phase [21]. This means that these crystals have never undergone any phase transition. Thus the influence of strains and stresses associated with the successive phase transitions has not been taken into account in such studies.

On the contrary, the manufacturing of zirconia-based *bulk* materials usually requires high temperature processes. In

*Author to whom correspondence should be addressed: rene.guinebretiere@unilim.fr

 

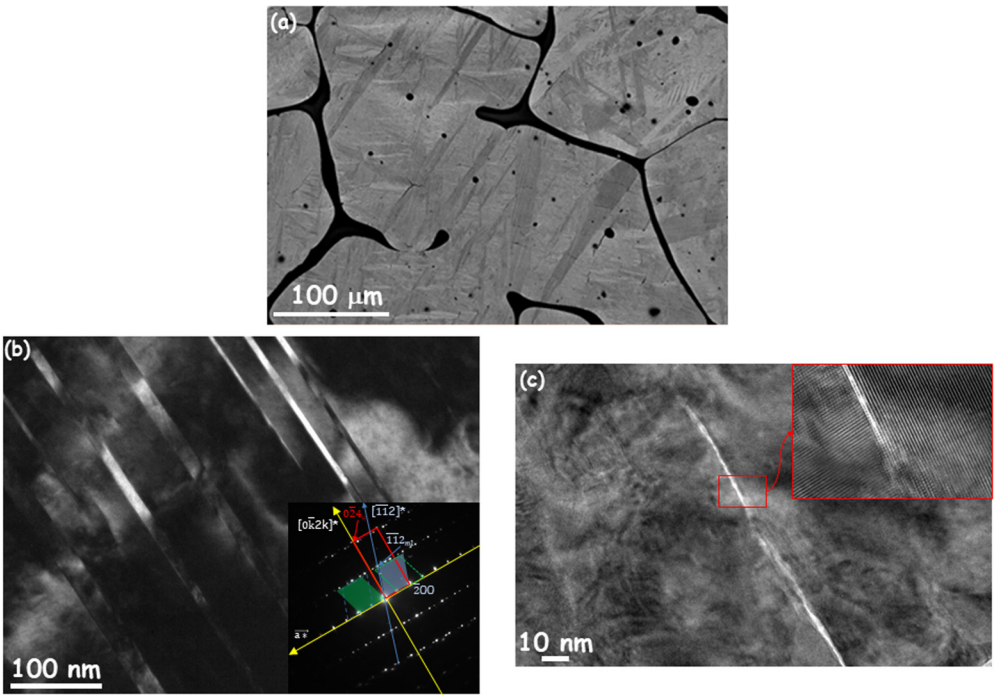


FIG. 1. Room temperature observations through electron microscopy of the microstructure of the studied material. (a) SEM micrograph evidencing the global microstructure of the material. Submillimetric areas embedded in a glassy phase (dark grey) are made of a very large number of monoclinic pure zirconia crystals (grey). (b) Twinning observed through dark field imaging by transmission electron microscopy (TEM). (c) TEM observation of a microcrack.

fact, dense zirconia materials are most often obtained by sintering and, in some cases, through fuse casting. Temperatures higher than 1200 °C are necessary, and both processes are associated with at least the $t \rightarrow m$ SPT during the cooling of the materials. Our goal in this paper is to study the coupling between strain promoted by the volume variation linked to $t \rightarrow m$ SPT and the occurrence of this phase transition in dense pure zirconia polycrystals. Throughout this work, we consider polycrystalline samples that are free of external stresses.

We measured by *in situ* x-ray diffraction (XRD) experiments the evolution of the monoclinic and tetragonal volume fractions and simultaneously the crystal volume variations over a large temperature range. This allows us to quantitatively analyze these size-strain-SPT coupled evolutions. The volume expansion associated with the $t \rightarrow m$ transition induces elastic strains in the zirconia crystals that promote the appearance of x-ray diffuse scattering. We clearly show that the strain relaxation associated with the reverse $m \rightarrow t$ SPT results in a dramatic decrease in the diffuse scattering signal. From the experimental point of view, the implementation of this approach encounters two main difficulties. First of all, the temperatures under consideration are typically higher than 1000 °C. Quantitative XRD measurements at such high temperatures are challenging. The second point concerns the samples themselves. Bulk pure zirconia samples are mandatory to investigate the effects of internal stresses. It is well known that the $t \rightarrow m$ transition during the cooling of pure zirconia dense samples often leads to the breakage of the material associated with a relaxation of part of the internal stresses and, thus, to the disappearance of the stress effect we want to evaluate. Thanks to a collaboration with the Saint Gobain company, we have obtained pure zirconia samples that keep their integrity up to room temperature.

## II. MATERIALS AND METHODS

The dense bulk pure zirconia samples that we studied come from large submetric refractory blocks used for the building of continuous ovens devoted to the industrial manufacturing of glass. They are produced by the Saint-Gobain company using the fused-casting method. The full description of the manufacturing process and the resultant microstructure is beyond of the scope of the present paper; it has already been presented in a previous paper [22]. The raw materials contain roughly 95 wt% zirconia and 5 wt% silicon oxide. After melting, in the liquid state, due to the presence of a miscibility gap in the pseudobinary $ZrO_2$-$SiO_2$ phase diagram [23,24], two different compounds are present, i.e., pure zirconia crystals and a silica based glassy phase. As shown in previous studies, the solubility of silicon in zirconia is, in fact, roughly nil [25]. Consequently, cooling and solidification induce the formation of a material containing large areas of pure zirconia embedded in a silica-based glass [22] [see scanning electronic microscopy (SEM) image reported in Fig. 1(a)]. These submillimetric areas contain a very large number of constituting crystals. We have already shown [26] that each of these areas correspond to only one cubic crystal at high temperature. It means that all the monoclinic submicrometric crystals are all variants resulting from the two successive SPTs, i.e,. $c \rightarrow t$ and $t \rightarrow m$, occurring during the cooling of the sample. All the 24 theoretically possible variants are

present [26], and the size of the coherent domains is typically a few tens of nanometers [27]. The two SPTs are associated with an intensive twinning process that is illustrated in Fig. 1(b). As an example, an area containing both tetragonal (narrows) and monoclinic (wide) plates is observed under the $[\bar{1}20]^*$ zone axis. The aim of this paper is not to study the twinning process in monoclinic zirconia that has been already described [16]. Nevertheless, this observation illustrates the fact that the martensitic $t \rightarrow m$ SPT is not complete even at room temperature. The presence of microcracks, certainly due to the release of the stresses created by the volume expansion associated with the $t \rightarrow m$ SPT, is illustrated in Fig. 1(c) at the nanoscale.

A volume of matter corresponding to the area observed in Fig. 1(a) and, thus, to a unique parent cubic crystal constitutes an ideal sample allowing the evaluation of the impact on the SPT of elastic strains generated by the successive SPTs associated with the volume variations and with the anisotropic thermal expansion of monoclinic zirconia [28,29]. We recently determined the strain distribution in such samples using a local x-ray microdiffraction method [27,30]. A statistically representative volume was scanned step by step, and each submicrometric probed volume contained a large number of nanosized coherently diffracting domains. At room temperature, these domains are monoclinic, and we measured local deviatoric strains of a few percent (and up to 10%) in these pure zirconia crystals [27]. According to the elastic properties of monoclinic zirconia [31–34], this corresponds to local deviatoric stresses lying in the GPa range while the global average of the stress in the full volume is at least one order of magnitude smaller [27]. Huge stress gradients (GPa/$\mu$m) were also measured. One of the open questions that we address in the present article is the evolution of this strain state as a function of temperature. For that purpose, we investigate a specimen that has been heated *in situ* up to 1435 °C and then cooled down to room temperature. During this cycle, microcracks form and therefore the specimen microstructure evolves.

The simultaneous evolutions of the tetragonal to monoclinic zirconia volume fraction and of the thermal expansion of zirconia crystals as a function of temperature were determined by *in situ* XRD experiments done at the D2AM beamline [35] at the European Synchrotron Radiation Facility (ESRF), Grenoble (France). The XRD patterns were collected at 17.9 keV just below the zirconium absorption edge using a two-dimensional (2D)-pixel hybrid detector (XPAD 3.2, 560 × 960 pixels, pixel size 130 $\mu$m [36]) located ∼420 mm away from the sample, allowing for the entire part of the reciprocal space of interest to be recorded without any rotation of the detector. Each of the 2D diffraction patterns was recorded in 30 s. The $Q$ space was calibrated according to the measurement of a diffraction pattern of the NIST SRM 660c $LaB_6$ powder. All 2D XRD images were radially integrated using the pyFAI library [37] in order to reconstruct 1D diffraction patterns. Quantitative analyses of the diffraction signal were done on these integrated 1D patterns. Taking into account both the energy and the incidence angle (6°) of the x-ray beam, the penetration depth of the x rays was close to 100 $\mu$m. The optics of the beamline were optimized in order to get a monochromatic parallel beam with a width of 200 $\mu$m and a height of 20 $\mu$m such that the imprint of the beam on the sample was a square with an area of roughly 200 $\mu$m × 200 $\mu$m. Finally, the probed volume was roughly equal to that of one dendrite. Consequently, all the diffracting crystals come from the same cubic parent crystal. The cell parameters were determined through full pattern matching using the FULLPROF software [38], while the evolution of the monoclinic to tetragonal ratio was followed by peak by peak diffraction line fitting of the $\bar{1}11_m$, $111_m$, and $111_t$ Bragg reflections using a pseudo-Voigt function and taking into account all the structural and geometrical parameters [39].

On the experimental point of view, the key point was to be able to record the diffraction patterns *in situ* at temperatures high enough to promote the $m \rightarrow t$ SPT of all the zirconia crystals. For that purpose, we used the QMAX furnace installed on the D2AM beamline which allows for the realization of x-ray scattering experiments at temperatures up to 1700°C [29]. The bulk samples were put on the top of the furnace, which is designed in such a way that all the diffuse or diffracted x-ray beams emitted in the half space above the sample surface can be recorded by the detector. Temperature variations induce thermal expansion not only of the sample but also of some parts of the heating sample holder; consequently the sample surface shifts. Therefore, the entire furnace is located on top of the goniometer head so that after reaching each target temperature, the sample surface was fully realigned prior to the measurement of the diffraction patterns. This allows the well-known sample displacement problem to be solved [40]. More information concerning this procedure can be found in [29].

Another challenging point during the *in situ* high temperature measurements is the determination of the true value of the temperature. The actual temperature of interest is, of course, not the temperature of the resistor nor the expected temperature with respect to the applied electrical power but the temperature of the sample. Before the experiment, a thin layer of NIST SRM 676a alumina powder was spread onto the bulk sample surface and we determined the sample temperature according to the thermal evolution of both the $a$ and $c$ cell parameters of $\alpha$ alumina [41].

## III. RESULTS AND DISCUSSION

### A. Phenomenological description of the $m \Leftrightarrow t$ phase transition process

We study the phase transition process in a constant volume probed by the x-ray beam. Considering that the x-ray penetration depth is close to 100 $\mu$m, according to the geometrical characteristics of the primary beam (see above), the probed volume during the XRD measurements is roughly 200 $\mu$m × 200 $\mu$m × 100 $\mu$m = $4 \times 10^6$ $\mu m^3$. According to the submicrometric size of the diffracting crystals, their number is sufficiently high to allow a statistical approach of the diffraction signal [39]. The actual sample is, in fact, this probe volume that contains all the 24 monoclinic variants associated with the two successive SPTs. Since the formal submillimetric cubic crystals [grey regions in Fig. 1(a)] at high temperature are mechanically disconnected due to the low viscosity of the $SiO_2$ glassy matrix, and therefore submitted to a small

average external stress, the study of one of these volumes corresponding to one formal cubic crystal is representative of the whole specimen.

During temperature variations, because the highest considered temperature is well below the melting temperature of zirconia, and assuming the absence of any stoichiometry variation of zirconia, the total number of $ZrO_2$ molecules is kept constant in the probed volume. The crystal volume evolutions are the variations of the volume occupied by these molecules.

At a given temperature $T$, the mean volume occupied by each $ZrO_2$ molecule in the zirconia crystals is equal to

$$\langle V(T)\rangle = \tau^t(T)\langle V^t(T)\rangle + [1-\tau^t(T)]\langle V^m(T)\rangle, \quad (1)$$

where $\tau^t(T)$ is the volume fraction of tetragonal zirconia at temperature $T$, and $\langle V^t(T)\rangle$ and $\langle V^m(T)\rangle$ are the mean volumes occupied by one molecule of $ZrO_2$ in the tetragonal and monoclinic zirconia crystals, respectively. In both cases, the average is expressed over all of the diffracting tetragonal or monoclinic crystals present in the probed volume.

As previously indicated, tetragonal zirconia crystallizes under the $P4_2/nmc$ space group. Nevertheless, this structure is commonly described in the pseudocubic "face-centered-tetragonal" lattice in which the crystallographic directions are parallel to those of the cubic form (see, for example, [42]). This setting is very efficient to follow the $m \Leftrightarrow t$ phase transition process. Accordingly, we adopt it throughout this paper, and, in that case, the pseudocubic tetragonal cell and the monoclinic cell both contain four molecules of $ZrO_2$.

Equation (1) can thus be rewritten as a function of the volume of the tetragonal and monoclinic cells:

$$\langle V(T)\rangle = \tfrac{1}{4}\left\{\tau^t(T)\left\langle V_c^t(T)\right\rangle + [1-\tau^t(T)]\left\langle V_c^m(T)\right\rangle\right\}, \quad (2)$$

where $\langle V_c^t\rangle$ and $\langle V_c^m\rangle$ are the mean tetragonal and monoclinic cell volumes, respectively, averaged over all the diffracting tetragonal or monoclinic crystals. It is worth noting that these lattice volumes take into account not only the expansion of the lattice due to thermal dilation, e.g., as would be measured on a stress-free powder, but also the distribution of local stresses (expected to be in the GPa range [27]) inside the material.

According to basic thermodynamics, the thermal expansivity is expressed by the volume variation induced by an infinitesimal variation in the temperature. It is obtained by the derivative of Eq. (2) with respect to the temperature and is expressed as

$$\frac{\partial\langle V(T)\rangle}{\partial T} = \frac{1}{4}\left[\left(\frac{\partial\left\langle V_c^t(T)\right\rangle}{\partial T} - \frac{\partial\left\langle V_c^m(T)\right\rangle}{\partial T}\right)\tau^t(T) + \frac{\partial\left\langle V_c^m(T)\right\rangle}{\partial T}\right] + \frac{1}{4}\left[\frac{\partial\tau^t(T)}{\partial T}\left[\left\langle V_c^t(T)\right\rangle - \left\langle V_c^m(T)\right\rangle\right]\right].$$

The first part of the right member of this equation,

$$\frac{\partial V_1(T)}{\partial T} = \frac{1}{4}\left[\left(\frac{\partial\left\langle V_c^t(T)\right\rangle}{\partial T} - \frac{\partial\left\langle V_c^m(T)\right\rangle}{\partial T}\right)\tau^t(T) + \frac{\partial\left\langle V_c^m(T)\right\rangle}{\partial T}\right], \quad (3)$$

is closely related to the expansivity of the monoclinic and tetragonal cells for a given volume fraction $\tau^t$ and is, thus, connected with the thermal dilation and internal stress state. It will be denoted as the "pure thermal expansion effect." The second term,

$$\frac{\partial V_2(T)}{\partial T} = \frac{1}{4}\frac{\partial\tau^t(T)}{\partial T}\left[\left\langle V_c^t(T)\right\rangle - \left\langle V_c^m(T)\right\rangle\right], \quad (4)$$

is connected with the volume transfer between the $m$ and $t$ phases associated with a temperature variation. It will be denoted, hereafter, as the "phase transition thermal expansivity."

According to Eqs. (3) and (4), the quantitative knowledge of the variation in both tetragonal and monoclinic mean cell volumes together with the evolution of the volume fraction of tetragonal crystals allows the influence of the phase transition on the mean crystal volume variations as a function of the temperature to be determined. All these quantities can be extracted from the XRD patterns, as detailed below in Secs. III B and III C.

The evolution of the volume fraction of tetragonal zirconia $\tau^t(T)$ in the probed volume with temperature can be expressed according to a basic energy balance related to phase transition considerations. In fact, at a given temperature, a tetragonal crystal transforms to monoclinic if the Gibbs free energy gap $\Delta G^{t\to m}(T)$ between the two phases becomes negative. Assuming spherical particles, this free energy gap is classically written as

$$\Delta G^{t\to m}(T) = \tfrac{4}{3}\pi r^3\left[\Delta G_V^{tm}(T) + \Delta G_D(T)\right] + 4\pi r^2\Delta G_S^{tm}(T), \quad (5)$$

where $r$ is the radius of the crystal, $\Delta G_V^{tm}(T)$ is the difference between the volume free energy of a tetragonal and a monoclinic crystal of radius $r$, $\Delta G_D(T)$ is the free energy associated with the appearance of interfacial elastic strains, and $\Delta G_S^{tm}(T)$ is the difference between the surface free energy of a tetragonal and a monoclinic crystal of radius $r$. Accordingly, if one assumes that the transition is essentially driven by a size effect, the critical radius of the $t \to m$ transition of a crystal is given by

$$r_c^{t\to m}(T) = -\frac{3\Delta G_S^{tm}(T)}{\left[\Delta G_V^{tm}(T) + \Delta G_D(T)\right]}. \quad (6)$$

This means that at temperature $T$, all tetragonal crystals with a radius equal to $r_c^{t\to m}$ transform to monoclinic, while the larger tetragonal crystals have already transformed at higher temperatures.

Let's assume that at a temperature much higher than the start of the $t \to m$ transition, the size of the tetragonal crystals follows a log-normal distribution with parameters $\mu$ and $\sigma$,

$$f(r) = \frac{1}{r\sigma\sqrt{2\pi}}\exp\left[-\frac{1}{2}\left(\frac{\ln(r)-\mu}{\sigma}\right)^2\right].$$

Here, $\mu$ and $\sigma$ are the arithmetic mean and standard deviation of $\ln(r)$, respectively. The mean $\bar{r}$ and standard deviation $\bar{\bar{r}}$ of the size distribution are given, respectively, by

$$\bar{r} = \exp\left(\mu + \frac{\sigma^2}{2}\right), \quad \bar{\bar{r}} = \bar{r}[\exp(\sigma^2)-1]^{1/2}$$

and thus

$$\mu = \ln\left[\frac{\bar{r}^2}{\sqrt{\bar{r}^2+\bar{\bar{r}}^2}}\right], \quad \sigma^2 = \ln\left[\frac{\bar{r}^2+\bar{\bar{r}}^2}{\bar{r}^2}\right] \quad (7)$$

The associate cumulative distribution function, which expresses the volume fraction $\tau^t(T)$ of the tetragonal phase at temperature $T$, is given by

$$\tau^t(T) = \int_0^{r_c^{t\to m}(T)} f(r)dr = \frac{1}{2}\left[1 + \mathrm{erf}\left(\frac{\ln\left(r_c^{t\to m}(T)\right) - \mu}{\sigma\sqrt{2}}\right)\right].$$

For practical purposes, this expression can be simplified by using the approximation of the error function erf proposed in [43] [see Eq. (3.11) therein], which is sufficiently accurate for our application. This leads to

$$\tau^t(T) \simeq \frac{1}{1 + \exp\left[-\frac{4\tilde{r}_c^{t\to m}(T)\left(1+k(\tilde{r}_c^{t\to m}(T))^2\right)}{\sqrt{\pi}}\right]}, \quad (8)$$

where

$$\tilde{r}_c^{t\to m}(T) = \frac{\ln\left(r_c^{t\to m}(T)\right) - \mu}{\sigma\sqrt{2}} \quad (9)$$

is a normalized critical radius. The coefficient $k = 0.089\,430$ has been introduced in [43].

On the other hand, it will be shown in the next section that the experimental data are nicely fitted by a sigmoidal law

$$\tau^t(T) = \frac{1}{1 + \exp[-\lambda(T - T_c)]}, \quad (10)$$

where $T_c$ is the critical phase transition temperature in the sense of the Landau phase transition theory ($\tau^t_{T=Tc} = 0.5$) and $\lambda$ characterizes the "width" of the sigmoid. The numerator of (10) is equal to 1 as the transition can be complete. Then, identifying (8) and (10) leads to the following third order equation:

$$\left[\tilde{r}_c^{t\to m}(T)\right]^3 + \frac{1}{k}\tilde{r}_c^{t\to m}(T) - \frac{\sqrt{\pi}\lambda(T - T_c)}{4k} = 0, \quad (11)$$

which has a unique real solution that is written as (Cardan formula)

$$\tilde{r}_c^{t\to m}(T) = \sqrt[3]{\frac{-q + \sqrt{\Delta}}{2}} + \sqrt[3]{\frac{-q - \sqrt{\Delta}}{2}}, \quad (12)$$

where $p = \frac{1}{k}$, $q = -\frac{\sqrt{\pi}\lambda(T-T_c)}{4k}$, and $\Delta = q^2 + \frac{4}{27}p^3$.

In the following, the thermal dependence of the volume fraction of tetragonal zirconia is determined according to Eq. (10), and the phase transition thermal expansivity is evaluated according to Eq. (4).

### B. Quantitative experimental analysis of the phase transition process

We followed the evolution of $\tau^t(T)$ *in situ* in a bulk sample between room temperature and 1500°C during heating and cooling. Parts of the 1D diffraction patterns are reported in Figs. 2(a)–2(c). The $m \Leftrightarrow t$ phase transition is illustrated by the evolution of the diffraction signal in the $Q$ range close to the 1,1,1 reciprocal lattice nodes (RLNs). In fact, the splitting of the (111) tetragonal diffraction peak to the ($\bar{1}11$) and (111) peaks is characteristic of the formation of the monoclinic phase. Due to the volume expansion associated with the $t \to m$ transition, the cooling process is critical with respect to the microcrack formation. In the corresponding temperature range, diffraction patterns were recorded every 6°C [see Fig. 2(c)].

According to the phenomenological description of the relationship between the $m \Leftrightarrow t$ phase transition and the zirconia crystal size, we have fitted the evolution of the volume fraction of tetragonal zirconia assuming a sigmoidal evolution with respect to the temperature. The best fits that we obtained are reported in Figs. 2(d) and 2(e), and the values of the critical temperatures $T_c$ and $\lambda$ are indicated in Table I. In both cases, the critical temperatures are lower than the transition temperature of the pure zirconia perfect crystals free of any stress, which is reported to be equal to 1170°C. Moreover, one can see that the critical temperature of the $t \to m$ transition is 120°C below that of the $m \to t$ transition. Except at the beginning of the $t \to m$ SPT during cooling, the global evolution of the $\tau^t(T)$ follows the sigmoidal law quite well and this is consistent with the model in which the phase transition is essentially driven by size effects.

The evolution of the volume fraction of tetragonal zirconia during heating and cooling is reported in Fig. 2(f) as a function of the reduced temperature $T$-$T_c$. The reverse $t \to m$ transition during cooling is spread over a range of temperatures that is much wider than that observed for the $m \to t$ transition. In fact, the $m \to t$ SPT occurs in a temperature range of roughly 350°C, while the $t \to m$ SPT spreads over 1000°C. Both this feature and the critical temperature gap between heating and cooling are clear illustrations of the influence of the excess of free energy related to stresses induced by the increase in the $ZrO_2$ molecular volume associated with the $t \to m$ transition. This free energy excess is, of course, a function of the temperature, and it corresponds to the strain energy $\Delta G_D(T)$ in Eq. (5).

The evolution of the normalized critical radius $\tilde{r}_c^{t\to m}(T)$ as a function of the temperature can be plotted according to Eq. (12) at given $\lambda$ and $T_c$ values. The curve corresponding to the cooling process is reported in Fig. 3(a). The knowledge of the mean value and the standard deviation of the crystal size distribution is needed to determine the thermal evolution of the critical radius [see Eq. (8)]. It is not the aim of this paper to compare the evolution of the critical radius as a function of the characteristics of the crystal size distribution, i.e., the microstructure, which depends on the manufacturing process. Nevertheless, as an illustration, we have plotted in Fig. 3(b) the evolution of this critical radius for a mean crystal size of $\bar{r} = 100$ nm and two standard deviations, $\bar{\bar{r}} = 10$ nm and $\bar{\bar{r}} = 30$ nm. As expected, the obtained critical size increases with temperature with values in the 100-nm range. Interestingly, the critical size depends significantly on the initial size distribution, the fluctuation with temperature being much larger for the broader size distribution ($\bar{\bar{r}} = 30$ nm) of tetragonal crystals at high temperatures. The specific shape of the considered size distribution (e.g., normal vs log-normal distribution) is found to have only a little influence (details not shown here).

Of course, the values of $\lambda$ and $T_c$ are very strongly related to the microstructure and residual stress state of the material

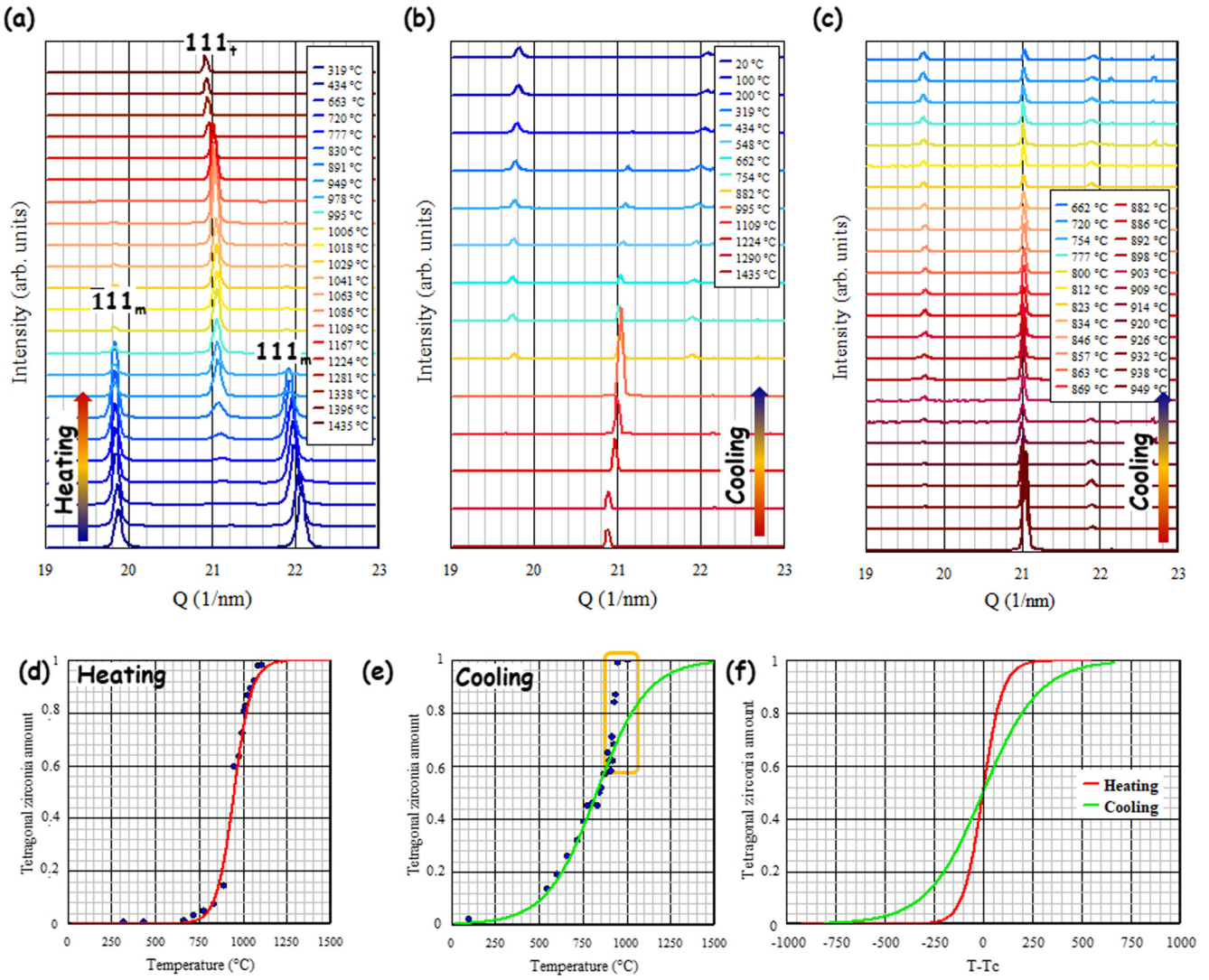


FIG. 2. Volume fraction of tetragonal zirconia as a function of temperature during heating and cooling. (a)–(c) Part of the XRD patterns recorded during the heating and cooling processes. During cooling, the diffraction patterns were recorded roughly every 6°C [see (c)]. (d),(e) Fit with a sigmoidal law of the evolutions of the volume fraction of tetragonal zirconia as a function of temperature during heating and cooling. (f) Evolution of the tetragonal volume fraction with respect to the critical $m \rightarrow t$ and $t \rightarrow m$ phase transition temperatures. Only the crystal size effect is considered in (f).

under consideration, which remains challenging to characterize at high temperatures. Nevertheless, we have shown that the evolution of the critical size associated with the SPT can be experimentally determined.

A peculiar behavior is observed at the beginning of the $t \rightarrow m$ SPT during the cooling process [see the orange rectangle in Fig. 2(e)]. In a very narrow range of temperature, between 950°C and 925°C, roughly 30 vol% of the tetragonal zirconia is transformed into monoclinic, and below this temperature, the evolution of $\tau^t(T)$ follows the sigmoidal law very well again. This behavior is discussed in more detail below, but it attests to the occurrence of an additional phenomenon superimposed to the size effect and promoting the $t \rightarrow m$ SPT of a significant part of the zirconia crystals.

TABLE I. Phase transition critical temperatures and "widths" of the sigmoid during heating and cooling.

| | Critical temperature $T_c$ (°C) | $\lambda$ (°C$^{-1}$) |
|---|---|---|
| Heating | 950 | 0.020 |
| Cooling | 830 | 0.007 |

### C. Phase transition, strain relaxation and diffuse scattering

According to Eq. (4), the determination of the phase transition thermal expansivity requires the determination of monoclinic and tetragonal mean cell volume expansions and, thus, of the cell parameters themselves. The evolutions as a function of the temperature of the monoclinic and tetragonal cell parameters are reported in Fig. 4. The thermal dependencies

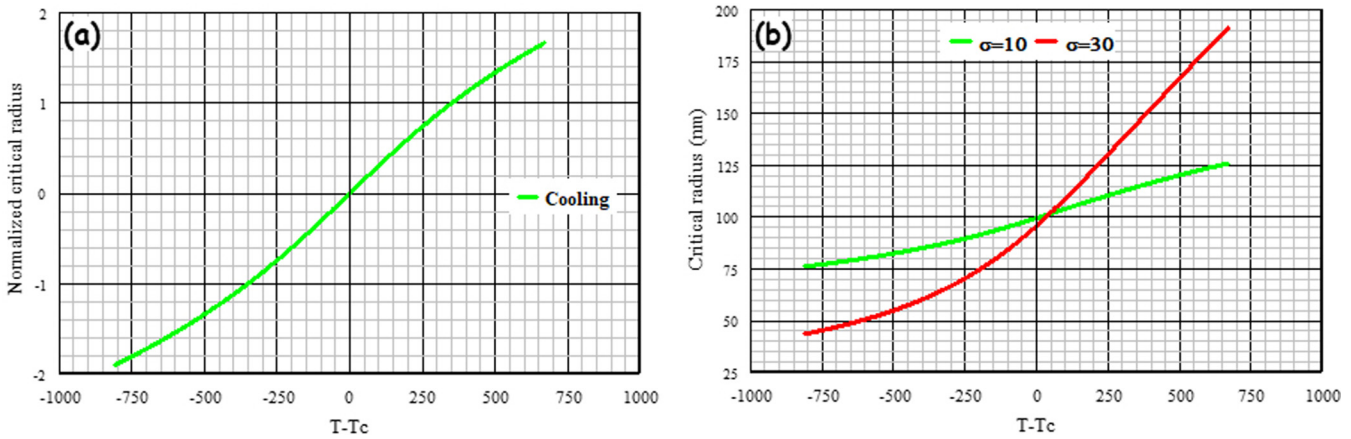


FIG. 3. Evolution of the critical crystal size for the $t \rightarrow m$ SPT during the cooling process. (a) The normalized critical radius is plotted according to Eq. (12) taking into account the value of λ and the critical temperature that have been determined experimentally for cooling (Table I). (b) Critical radius considering a hypothetical value of the mean crystal size (100 nm) and standard deviations of the size distribution of 10 and 30 nm.

of these cell parameters ($a_{t,m}$, $b_m$, $c_{t,m}$, $\beta_m$) were fitted by linear evolutions reported in Table II. The accordance of the experimental values and these linear laws is illustrated in Fig. 4. Note that the obtained lattice spacing evolutions account for both (i) the thermal dilation of the lattice, generally measured on stress free specimens such as powders, and (ii)

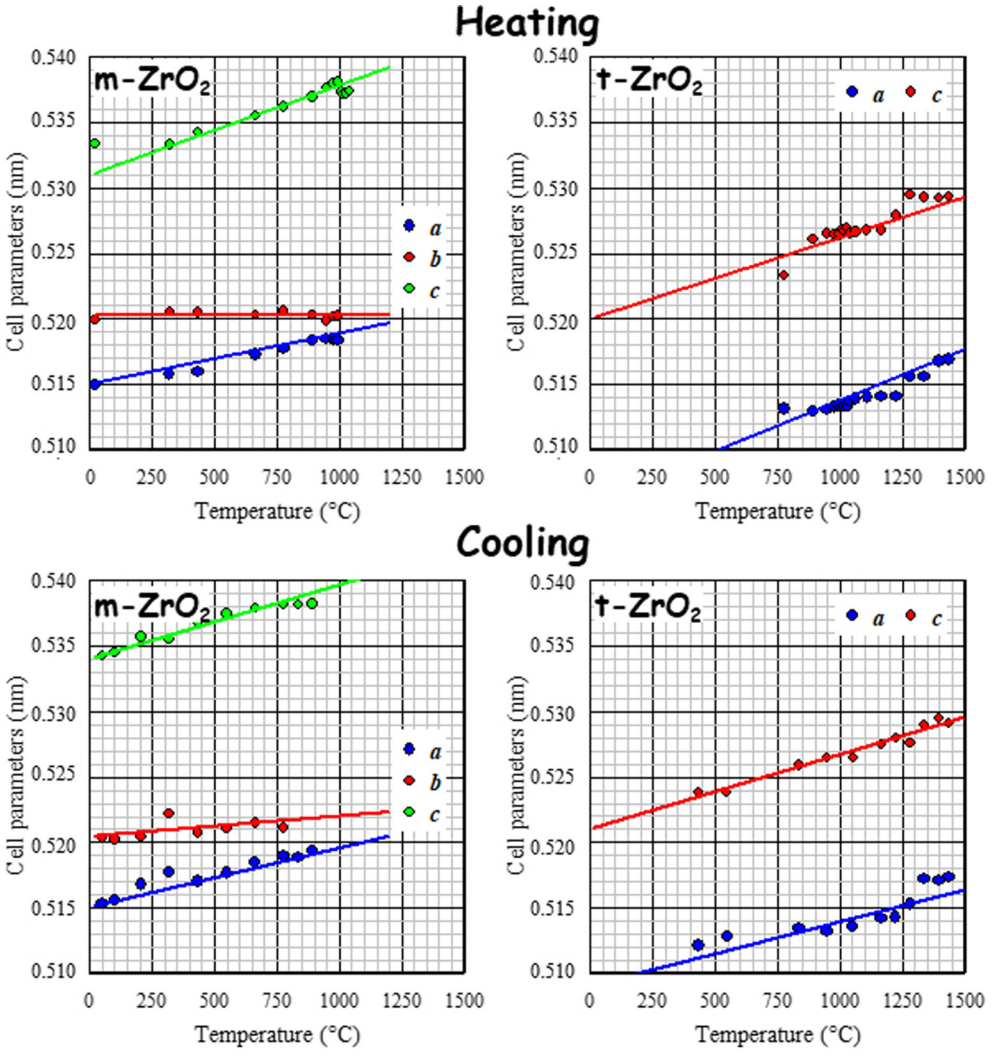


FIG. 4. Mean thermal expansion along the main crystallographic axis of the monoclinic and tetragonal crystals.

TABLE II. Linear evolution of the monoclinic and tetragonal cell parameters as a function of temperature (°C).

| | | | | Values from the literature obtained on pure zirconia powders | | | | |
|---|---|---|---|---|---|---|---|---|
| | | | | micrometric crystals | | nanosized crystals | | |
| | | Heating | Cooling | [44] | [45] | [46] | [47] | |
| $m$-$ZrO_2$ | $a_m$ (nm) | $0.515 + 3.90 \times 10^{-6}\,T$ | $0.515 + 4.54 \times 10^{-6}\,T$ | | $0.514 + 5.35 \times 10^{-6}\,T$ | | $0.515 + 4.18 \times 10^{-6}\,T$ | |
| | $b_m$ (nm) | $0.520 + 0.00 \times 10^{-6}\,T$ | $0.520 + 1.55 \times 10^{-6}\,T$ | | $0.520 + 0.81 \times 10^{-6}\,T$ | | $0.521 + 0.54 \times 10^{-6}\,T$ | |
| | $c_m$ (nm) | $0.531 + 6.85 \times 10^{-6}\,T$ | $0.534 + 5.66 \times 10^{-6}\,T$ | | $0.531 + 7.77 \times 10^{-6}\,T$ | | $0.531 + 6.84 \times 10^{-6}\,T$ | |
| | $\beta_m$ (deg) | $99.1 - 5.19 \times 10^{-4}\,T$ | $99.5 - 7.86 \times 10^{-4}\,T$ | | | | | |
| $t$-$ZrO_2$ | $a_t$ (nm) | $0.506 + 7.78 \times 10^{-6}\,T$ | $0.509 + 4.89 \times 10^{-6}\,T$ | $0.5074 + 6.36 \times 10^{-6}\,T$ | $0.509 + 5.64 \times 10^{-6}\,T$ | $0.506 + 6.91 \times 10^{-6}\,T$ | $0.509 + 5.16 \times 10^{-6}\,T$ | |
| | $c_t$ (nm) | $0.520 + 6.20 \times 10^{-6}\,T$ | $0.521 + 5.69 \times 10^{-6}\,T$ | $0.5188 + 7.57 \times 10^{-6}\,T$ | $0.517 + 8.51 \times 10^{-6}\,T$ | $0.514 + 10.30 \times 10^{-6}\,T$ | $0.520 + 6.36 \times 10^{-6}\,T$ | |

the internal stresses arising from the cooling and the phase transitions. This is because these lattice strains have been measured directly for the bulk specimen in which high internal stress is expected. Therefore, these lattice spacings are the actual *in situ* ones and can be used directly to compute the lattice volume as needed in Eqs. (3) and (4).

The first observation concerns the strong anisotropy of the thermal expansion of monoclinic zirconia. Indeed, in agreement with previous results obtained on pure zirconia powders [28,29], during heating the value of the $b$ cell parameter is quasi-independent of the temperature and only a slight evolution is observed during the cooling. Most of the previously published papers related to zirconia thermal expansion concern bulk or powdered materials made of doped zirconia, and because of the presence of residual stresses, different values of thermal expansion are expected for different samples. As the internal stress state in these specimens is largely unknown, comparison with our results is not relevant. Only a comparison with the thermal expansion of pure zirconia crystals almost free of external constraint could be useful. It is not the aim of the present paper to discuss in detail the evolutions of these cell parameters with respect to the values already published in the literature, nevertheless, we reported in Table II four data sets coming from the literature and more or less respecting this requirement.

The influence of the presence of residual stresses is evidenced by the discrepancy between the expansion coefficients measured during heating and cooling. Moreover, a reverse behavior is observed between the $a$ and $c$ axis of the monoclinic phase, i.e., the slope in Fig. 4 is higher during cooling than during heating along the $a$ axis while the opposite situation is observed along the $c$ axis. All these values are linked to the stress state and, more generally, to the microstructure of the sample. Here, the precise value of the lattice parameter is not of general interest as it depends on the internal stress state, which itself depends on the manufacturing process. For example, changing the cooling process a little will result in different values of the lattice parameters. However, according to the values reported in Table II, it is easy to calculate the difference in the molecular volume of zirconia under the monoclinic and tetragonal forms as a function of the temperature.

We have reported in Figs. 2(d) and 2(e) the evolution of the volume fraction of tetragonal zirconia modeled by sigmoidal laws corresponding to Eq. (10). The derivative of this volume fraction is thus given by

$$\frac{\partial \tau^t(T)}{\partial T} = \lambda[1 - \tau^t(T)]\tau^t(T). \tag{13}$$

Inserting this last expression into Eq. (4), the phase transition thermal expansivity during both heating and cooling can be estimated, as shown in Fig. 5(a). During heating, the $m \rightarrow t$ phase transition is associated with a diminution of the molecular volume of zirconia; this corresponds to a negative thermal expansivity. On the contrary, the $t \rightarrow m$ transition occurring during cooling induces a positive expansivity that is spread over a wide temperature range. The thermal expansion associated with this SPT results in an excess of free energy that induces both the decrease in the phase transition critical temperature and a spreading of the transition temperature.

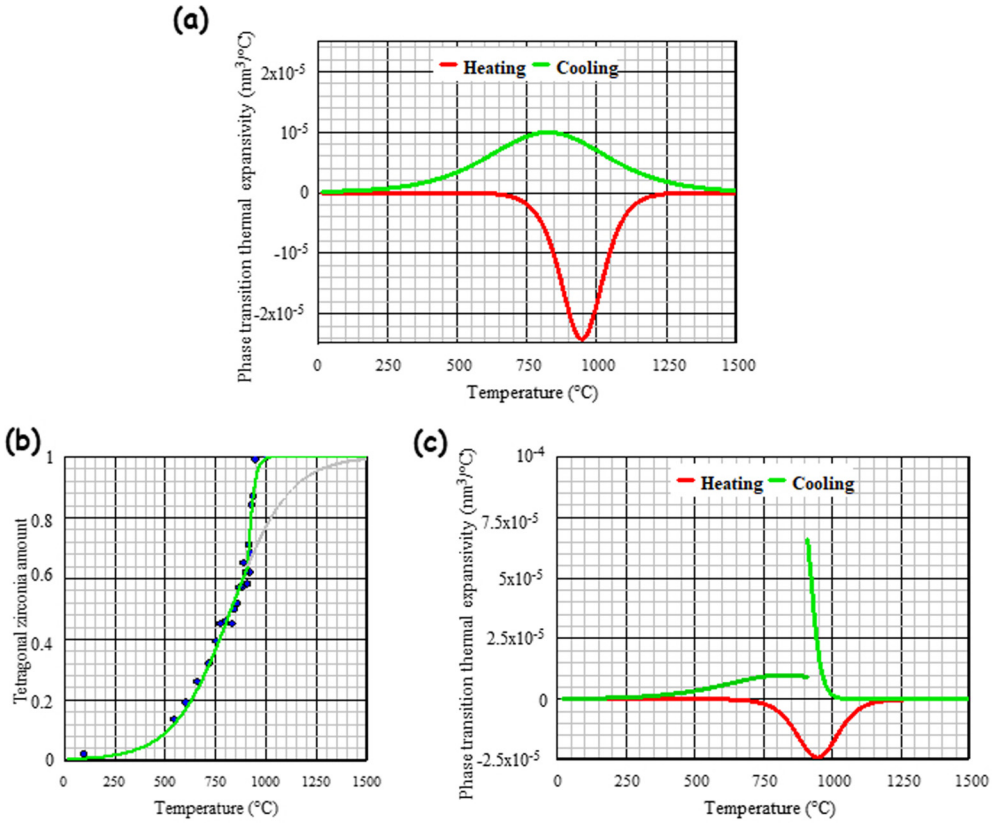


FIG. 5. Phase transition thermal expansivity. (a) Thermal expansivity during heating and cooling assuming a phase transition process fully driven by the size distribution of the crystals. (b) Modeling of the thermal variation of the volume fraction of tetragonal zirconia taking into account the sudden transition of 30 vol% of tetragonal zirconia at the beginning of the cooling process. (c) Phase transition thermal expansivity taking into account the true evolution of the amount of tetragonal zirconia.

The total elastic energy density associated with the phase transition, denoted hereafter as $E^{\rm tm}_{\rm elas}$, can be expressed as a function of the elastic strain field generated by the phase transition as

$$E^{\rm tm}_{\rm elas} = \int_{T_S}^{T_F} \Delta G_D(T)dT = \frac{1}{2}\int_{T_S}^{T_F} \langle \varepsilon_{ij} C_{ijkl} \varepsilon_{kl} \rangle dT. \quad (14)$$

Here, $\Delta G_D$ is the elastic energy stored or relaxed during the phase transition as introduced in Eq. (5), and it is integrated between the start ($T_S$) and finish ($T_F$) martensitic transformation temperatures. It accounts for the *elastic* strain field $\varepsilon_{ij}$ that is due to the sole phase transition, i.e., which is associated with the stress field resulting from the change in the lattice volume during the SPT. It does not account for the thermal dilation of the $t$ and $m$ phases. In Eq. (14), $C_{ijkl}$ are the components of the stiffness tensor at the crystal scale. Use is made of the Einstein summation convention over repeated indices, and the brackets $\langle . \rangle$ denote the volume average over the specimen volume. Neglecting the elastic anisotropy at the crystal scale, (14) becomes

$$E^{\rm tm}_{\rm elas} = \int_{T_S}^{T_F} \Delta G_D(T)dT = \frac{E}{2}\int_{T_S}^{T_F} \left[ \frac{1}{(1+\nu)} \langle \varepsilon'_{ij}\varepsilon'_{kl} \rangle + \frac{1}{3(1-2\nu)} \langle {\rm tr}(\varepsilon)^2 \rangle \right] dT, \quad (15)$$

where $\varepsilon'_{ij}$ is the deviatoric elastic strain and ${\rm tr}(\epsilon)$ is the trace of $\varepsilon$ expressing the *elastic part* of the lattice volume change during the phase transition. Experimental data on the elastic properties of the monoclinic and tetragonal pure zirconia near the $t \rightarrow m$ SPT are, in fact, not available. According to [31], the Young's modulus of monoclinic zirconia decreases slightly between room temperature and 1000°C. Its temperature variation evaluated experimentally by Chan *et al.* [31] depends on the model used for the extraction of this variation, but in all cases, variations are smaller than 10%, and as a first approximation, it can be considered quasiconstant as a function of the temperature and equal to ∼240 GPa with a Poisson ratio $\nu$ of ∼0.29. Theoretical calculations based on first principles studies have given values close to 200 GPa for the tetragonal polymorph [34]. As a first approximation, it can be assumed that the elastic properties of both the monoclinic and the tetragonal polymorphs near the $t \rightarrow m$ SPT are similar. As the response of the material is essentially elastic, and according to Eshelby's work [48,49], the elastic strain and stress fields inside the crystals generated by the SPT can be considered proportional to the lattice volume change during the SPT, which itself constitutes the main contribution to the phase transition thermal expansivity $V_2$ defined in (4). Accordingly, the stored elastic energy (15) is, as a first approximation, proportional to the integral of the square of the green curve reported in Fig. 5(a). Following this approach, it is worth noting that $E^{t\rightarrow m}_{\rm elas}$ stored during the cooling process

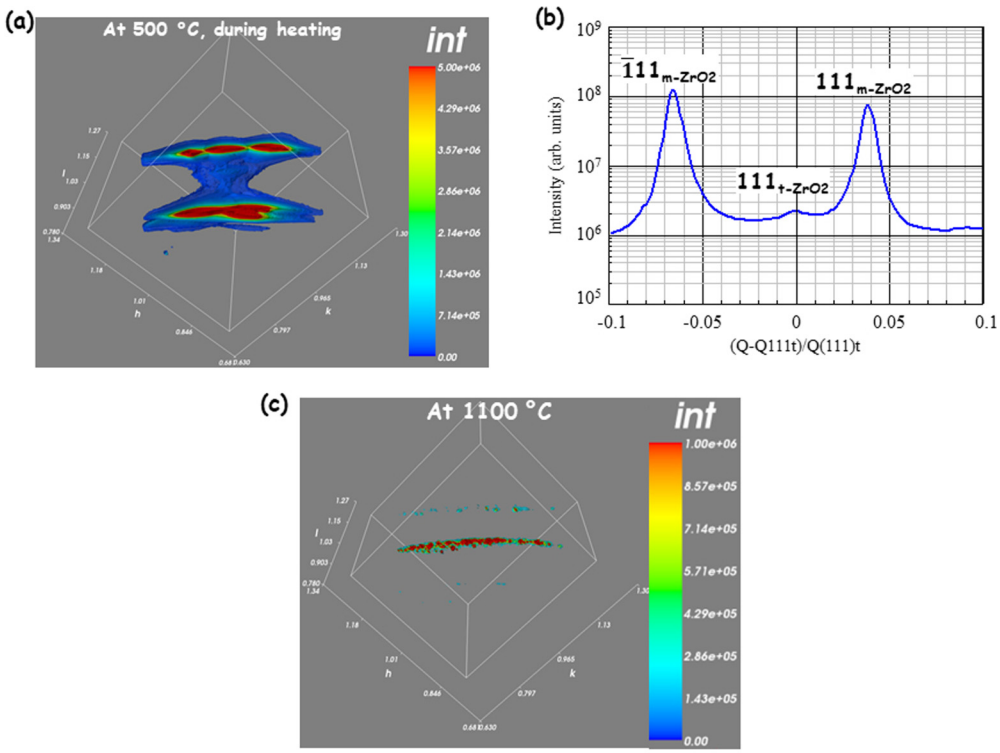


FIG. 6. Phase transition and diffuse scattering probed by 3D reciprocal space mapping close to the 1,1,1 zirconia tetragonal and monoclinic RSNs. (a) 3D-RSM recorded at 500°C during heating. (b) 1D pattern obtained by integration over the azimuthal and tilt angles of the intensity distribution reported in Fig. 5(a). (c) 3D-RSM recorded during heating at 1100°C.

is two times higher than $E_{\text{elas}}^{m\rightarrow t}$ relaxed during the reverse process. Thermal cycling of the material, thus, seems to induce a significant storage of elastic energy.

As shown in Fig. 2, the situation is, in fact, more complex. The green curves reported in Figs. 2(e) and 4(a) do not consider the sudden decrease in the volume fraction of tetragonal zirconia between 950°C and 925°C. Within 25°C, roughly 30 vol% of the tetragonal zirconia is transformed to monoclinic. Modeling of this evolution allows the phase transition thermal expansion associated with this very sudden evolution to be estimated [see Fig. 5(c)]. The highest value is typically one order of magnitude larger than the maximum reported in Fig. 5(a). In our dense bulk material, the transforming crystals are surrounded by other zirconia crystals, and the associated very large level of internal stresses cannot be accommodated by elastic deformation of those crystals. The discontinuity observed in Fig. 5(c) illustrates a sudden relaxation of the stress generated by the volume expansion associated with the $t \rightarrow m$ transition. This relaxation corresponds to the formation of microcracks and can be considered as a plastic relaxation.

Except for this part of the process, the high value of the phase transition thermal expansivity must be associated with a large level of stress inside the zirconia crystals. We have previously described the mean cell volume variations as a function of the temperature. Nevertheless, according to the theory of elasticity in solids, the presence of strains results in an *a priori* continuous variation of the $d$ spacing inside the crystal. In terms of x-ray diffraction, this must correspond to the spreading of the diffracted intensity near the central position of the considered reciprocal space nodes (RSNs). A continuous distribution of the $d$ spacing is associated, in the reciprocal space, with a continuous diffuse scattering signal. We have illustrated this feature by x-ray diffuse scattering measurements around the 1,1,1 monoclinic and tetragonal RSNs.

The probed volume is polycrystalline; nevertheless assuming that all the diffracting crystals belong to only one cubic parent crystal, the relative orientation of all the diffracting crystals is fully defined by the two successive SPTs. Considering the 1,1,1 RLN corresponding to the diffraction of crystals belonging to one common variant, it is quite easy to find in the reciprocal space another RLN associated with this set of diffracting crystals. After the determination of the position of the 1,1,1 and 2,0,0 $t$-$ZrO_2$ RLNs, we have used this approach to define a global orientation matrix of a set of crystals belonging to the same variant. We have then mapped in three dimensions the reciprocal space close to the central position of the 1,1,1 $t$-$ZrO_2$ RLN through the recording of 200 2D diffraction maps at each temperature. The 3D reciprocal space maps (RSMs) were reconstructed using a Python routine developed at the beamline. The total duration of the 3D mapping at each temperature was close to one hour.

The 3D RSM around the 1,1,1 nodes recorded at 500°C during the heating of the sample is reported in Fig. 6(a). First of all, a threefold picture clearly appears both for the $1, 1, 1_m$ and the $\bar{1}, 1, 1_m$ nodes. Such an observation illustrates the loss of the threefold axis of the initial cubic ⟨111⟩ directions. The split of the $1, 1, 1_t$ node into the $\bar{1}, 1, 1_m$ and $1, 1, 1_m$ nodes results from a twinning process. The diffuse scattering signal is clearly spread continuously between the opposite

monoclinic nodes and passes through the tetragonal 1,1,1 node. Because the spreading of diffuse scattering is very large, the contributions associated with each split node are partially superimposed to each other. We have integrated the whole signal with respect to the azimuthal and tilt angles [see Fig. 6(b)]. A large diffuse signal joining the three nodes is observed. Because the diffracting crystals are made of pure zirconia, the diffuse scattering signal cannot be due to any compositional fluctuation; it corresponds to a distribution of the (111) and ($\bar{1}$11) $d$-spacing values induced by elastic strains. The plot reported in Fig. 6(b) is centered on the position of the $t$-$ZrO_2$ RLN. A continuous distribution of $d$ spacing between the $\bar{1}$, 1, $1_m$ and the 1, 1, $1_m$ nodes corresponds to elastic strains of roughly 10%. It is interesting to note that such a value is in full agreement with local strain measurements obtained by Laue microdiffraction on the same sample at room temperature [26].

The 3D-RSM recorded at 1100°C during the heating process is reported in Fig. 6(c). At 1100°C, according to the 1D patterns drawn in Fig. 2(a), the signal is strongly dominated by the diffraction of tetragonal crystals. The diffuse scattering signal is much weaker than the one recorded at 500°C [note that the color scale is five times smaller than that used in Fig. 6(a)]. The negative thermal expansivity associated with the $m \rightarrow t$ transition [see Fig. 5(a)] induced a strong relaxation of the strains and the tetragonal crystals are, at this stage, at a much lower stress level compared to the monoclinic ones at 500°C before the $m \rightarrow t$ SPT.

## IV. CONCLUSIONS

It is well known that the mechanical properties of zirconia-based materials are strongly linked to the $m \Leftrightarrow t$ phase transition. At the microscopic scale, two different processes are responsible for the transformation toughening observed in such materials [16]. Macrocracks induced by mechanical external constraints promote relaxation of stresses around metastable tetragonal crystals that are suddenly transformed into the stable monoclinic form. The consumption of this transformation energy results in a decrease in the energy of propagation of the crack and thus slows down this propagation. The second process is related to the formation of microcrack networks around the monoclinic zirconia crystals appearing from crystals exhibiting a higher symmetry. In this process, the crystal volume variations associated with the $t \rightarrow m$ SPT and the formation of microcracks is strongly linked. However, these are two different phenomena that develop over *a priori* different temperature ranges. The aim of this paper is to disentangle the phase transition and microcracking processes through *in situ* high temperature x-ray diffraction measurements.

The temperature of the $m \Leftrightarrow t$ phase transition in pure zirconia perfect crystals is reported as 1170°C in the literature [1]. In fact, in actual dense ceramic materials, the situation is very different. We show experimentally that in a polycrystalline sample of pure zirconia, this phase transition spreads over a very large temperature range, which can be as large as 1000°C. Using a phenomenological description of the energy balance with respect to the crystal sizes, we fully explained this observation at a quantitative level.

As we have already shown by Laue microdiffraction experiments [27], the local strain generated by the SPT are of few percent, and considering the elastic properties of zirconia, such very high values correspond to stresses lying in the GPa range. During sample cooling, roughly a third of the tetragonal zirconia crystals are suddenly transformed into monoclinic crystals in a very narrow temperature range of only 25°C. This is clearly due to the huge and heterogeneous stress level that induces microcracking that partially relaxes this internal stress. Indeed, while the phase transition process occurs over a temperature range in the order of 1000°C, the main microcracking process occurs within only 25°C, and below this temperature range, the transformation process follows the law corresponding to a crystal size control of this phase transition.

All of the phase transition process occurs here out of equilibrium. Tetragonal pure zirconia crystals are still present at temperatures 1000°C below the theoretical phase transition temperature. We show that this is due to a subtle energy balance related to the crystal size, crystal volume variation, and local strain in zirconia crystals. As written in the Introduction, it is well known that the $m \Leftrightarrow t$ phase transition in a zirconia perfect single crystal is a first order one. A strong volume variation is observed at this transition. Nevertheless, considering a zirconia polycrystal made of an assembly of a large number of zirconia crystals characterized by a quite large size distribution in the submicrometer range and taking into account the high internal stresses in the material due to its manufacturing method, it appears that the phase transition, in fact, corresponds to a continuous volume variation [see Fig. 4(a)]. Such a smooth phase transition process associated with strain relaxation has already been described formally in polycrystals subjected to SPTs [50]. In fact, in the narrow temperature range in which the microcrack network quickly develops, the martensitic phase transition process corresponds to a first order SPT. On the contrary, at lower temperature the continuous volume variation corresponds, at the polycrystalline specimen scale, to a *second order phase transition process* for the large set of the transforming crystals. Such an evolution from a first order to a second order phase transition process has already been proposed when the SPT occurs in polycrystals under a stress field [50,51]. Recently, it has been evidenced through molecular dynamic calculations in the case of the martensitic transformation of a nickel-aluminum alloy under epitaxial stress [51]. Our experimental results are an illustration of a similar process in the case of the martensitic phase transition in a polycrystalline oxide dense material. In that case, the stress field is generated during the manufacturing process due to the anisotropic thermal expansion and SPTs during the cooling after the manufacturing of the material. Finally, it is worth noting that this quite smooth volume variation over a large temperature range probably explains the conservation of the integrity of the whole large specimens.

## ACKNOWLEDGMENTS

This work was performed within the framework of the ASZTECH and HoTMiX research programs, funded by the ANR (Grant No. ANR-12-RMNP-0007) and cofunded by the ANR and DFG (Grant No. ANR-19-CE09-0035), respectively. We acknowledge the ESRF and the French

Collaborating Research Group (F-CRG) for the provision of the synchrotron radiation facilities beamtimes. The authors are thankful to I. Cabodi and O. Bories (Saint-Gobain CREE) for the supply of the bulk zirconia-based materials and P. Carles from the electronic microscopy facility at IRCER for the realization of the TEM observations.

[1] M. Smirnov, A. Mirgorodsky, and R. Guinebretière, Phenomenological theory of lattice dynamics and polymorphism of $ZrO_2$, Phys. Rev. B **68**, 104106 (2003).

[2] O. Ohtaka, T. Yamanaka, S. Kume, E. Ito, and A. Navrotsky, Stability of monoclinic and orthorhombic zirconia: Studies by high-pressure phase equilibria and calorimetry, J. Am. Ceram. Soc. **74**, 505 (1991).

[3] G. M. Wolten, Diffusionless phase transformations in zirconia and hafnia, J. Am. Ceram. Soc. **46**, 418 (1963).

[4] G. K. Bansal and A. H. Heuer, On a martensitic phase transformation in zirconia ($ZrO_2$)–I. Metallographic evidence, Acta Metal. **20**, 1281 (1972).

[5] G. K. Bansal and A. H. Heuer, On a martensitic phase transformation in zirconia ($ZrO_2$)–II. Crystallographic aspects, Acta Metall. **22**, 409 (1974).

[6] R. C. Garvie, R. H. Hannink, and R. T. Pascoe, Ceramic steel? Nature (London) **258**, 703 (1975).

[7] P. Li, U. Wei Chen, and J. E. Penner-Hahn, Effect of dopants on zirconia stabilization–An X-ray absorption study: I, Trivalent dopants, J. Am. Ceram. Soc. **77**, 118 (1994).

[8] P. Li, U. Wei Chen, and J. E. Penner-Hahn, Effect of dopants on zirconia stabilization–An X-ray absorption study: II, Tetravalent dopants, J. Am. Ceram. Soc. **77**, 1281 (1994).

[9] P. Li, U. Wei Chen, and J. E. Penner-Hahn, Effect of dopants on zirconia stabilization–An X-ray absorption study: III, charge compensating dopants, J. Am. Ceram. Soc. **77**, 1289 (1994).

[10] T. Charaska, A. H. King, and C. C. Berndt, On the size dependent phase transformation in nanoparticulate zirconia, Mater. Sci. Eng. A **286**, 169 (2000).

[11] E. Djurado, P. Bouvier, and G. Lucazeau, Crystallite size effect on the tetragonal-monoclinic transition of undoped nanocrystalline zirconia studied by XRD and Raman spectrometry, J. Solid State Chem. **149**, 399 (2000).

[12] R. Guinebretière, Z. Oudjedi, B. Soulestin, and A. Dauger, Semi-coherent zirconia inclusions in a ceramic matrix, J. Mater. Res. **15**, 2482 (2000).

[13] A. Boulle, Z. Oudjedi, R. Guinebretière, B. Soulestin, and A. Dauger, Ceramic nanocomposites obtained by sol-gel coating of submicron powders, Acta Mater. **49**, 811 (2001).

[14] G. Baldinozzi, D. Simeone, D. Gosset, and M. Dutheil, Neutron Diffraction Study of the Size Induced Tetragonal to Monoclinic Phase Transition in Zirconia Nanocrystals, Phys. Rev. Lett. **90**, 216103 (2003).

[15] L. L. Lange, Transformation toughening, J. Mater. Sci. **17**, 225 (1982).

[16] P. M. Kelly and L. R. Francis Rose, The martensitic transformation in ceramics–its role in transformation toughening, Prog. Mater. Sci. **47**, 463 (2002).

[17] P. Aldebert and J. P. Traverse, Structure and ionic mobility of zirconia at high temperature, J. Am. Ceram. Soc. **68**, 34 (1985).

[18] R. C. Garvie, The occurrence of metastable tetragonal zirconia as a crystallite size effect, J. Phys. Chem. **69**, 1238 (1965).

[19] F. Boscherini, F. D'Acapito, S. F. Galata, D. Tsoutsou, and A. Dimoulas, Atomic scale mechanism for the Ge-induced stabilization of the tetragonal, very high-$K$, phase of $ZrO_2$, Appl. Phys. Lett. **99**, 121909 (2011).

[20] J. Müller, T. S. Böcke, U. Schröder, S. Müller, D. Bräuhaus, U. Böttger, L. Frey, and T. Mikolajick, Ferroelectricity in simple binary $ZrO_2$ and $HfO_2$, Nano Lett. **12**, 4318 (2012).

[21] R. Guinebretière, A. Dauger, A. Lecomte, and H. Vesteghem, Tetragonal zirconia powders from the Zr n-propoxide - acetylacetone - water - isopropanol system, J. Non-Cryst. Solids **147**, 542 (1992).

[22] C. Patapy, M. Huger, T. Chotard, R. Guinebretière, N. Gey, A. Hazotte, and M. Humbert, Solidification structure in pure zirconia liquid molten phase, J. Eur. Ceram. Soc. **33**, 259 (2013).

[23] H. Kin and P. C. McIntyre, Spinodal decomposition in amorphous metal-silicate thin films: Phase diagram analysis and interface effects on kinetics, J. Appl. Phys. **92**, 5094 (2002).

[24] A. Gaudon, A. Dauger, A. Lecomte, B. Soulestin, and R. Guinebretière, Phase separation in sol–gel derived $ZrO_2$-$SiO_2$ nanostructured materials, J. Eur. Ceram. Soc. **25**, 283 (2005).

[25] L. Gremillard, T. Epicier, J. Chevalier, and G. Fantozzi, Microstructural study of silica-doped zirconia ceramics, Acta Mater. **48**, 4647 (2000).

[26] M. Humbert, N. Gey, C. Patapy, E. Joussein, M. Huger, R. Guinebretière, and T. Chotard, and A. Hazotte, Identification and orientation determination of parent cubic domains from EBSD maps of monoclinic pure zirconia, Scr. Mater. **63**, 411 (2010).

[27] T. Ors, F. Gouraud, V. Michel, M. Huger, N. Gey, J. S. Micha, O. Castelnau, and R. Guinebretière, Huge local elastic strains in bulk nanostructured pure zirconia materials, Mater. Sci. Eng. A **806**, 140817 (2021).

[28] F. Frey, H. Boysen, and T. Vogt, Neutron powder investigation of the monoclinic to tetragonal phase transformation in undoped zirconia, Acta Crystallogr., Sect. B **46**, 724 (1990).

[29] R. Guinebretière, S. Arnaud, N. Blanc, N. Boudet, E. Thune, D. Babonneau, and O. Castelnau, Full reciprocal space mapping up to 2000 K under controlled atmosphere: The multi-purpose QMAX furnace, J. Appl. Cryst. **53**, 650 (2020).

[30] T. Örs, J. S. Micha, N. Gey, V. Michel, O. Castelnau, and R. Guinebretière, EBSD-assisted Laue microdiffraction for microstrain analysis, J. Appl. Cryst. **51**, 55 (2018).

[31] S. K. Chan, Y. Fang, M. Grimsditch, Z. Li, M. V. Nevitt, W. M. Robertson, and E. S. Zouboulis, Temperature dependence of the elastic moduli of monoclinic zirconia, J. Am. Ceram. Soc. **74**, 1742 (1991).

[32] A. P. Mirgorodsky and P. E. Quintard, Lattice-dynamic treatment of vibrational and elastic properties of cotunnite-type $ZrO_2$ and $HfO_2$: Comparison with ambient pressure polymorphs, J. Am. Ceram. Soc. **82**, 3121 (1999).

[33] X. S. Zhao, S. L. Shang, Z. K. Liu, and J. Y. Shen, Elastic properties of cubic, tetragonal and monoclinic $ZrO_2$ from first-principles calculations, J. Nucl. Mater. **415**, 13 (2011).

[34] G. Fadda, L. Colombo, and G. Zanzotto, First-principles study of the structural and elastic properties of zirconia, Phys. Rev. B **79**, 214102 (2009).

[35] G. A. Chahine, N. Blanc, S. Arnaud, F. de Geuser, R. Guinebretière, and N. Boudet, Advanced non-destructive *in situ* characterization of metals at the French CRG D2AM /BM02 beamline at the ESRF, Metals **9**, 352 (2019).

[36] https://www.esrf.fr/UsersAndScience/Experiments/CRG/BM02/detectors/xpad.

[37] G. Ashiotis, A. Deschildre, Z. Nawaz, J. P. Wright, D. Karkoulis, F. E. Picca, and J. Kieffer, The fast azimuthal integration Python library: PyFAI, J. Appl. Crystallogr. **48**, 510 (2015).

[38] J. Rodriguez Carvajal, Recent advances in magnetic-structure determination by neutron powder diffraction, Phys. B (Amsterdam, Neth.) **192**, 55 (1993).

[39] R. Guinebretière, *X-ray Diffraction on Polycrystalline Materials* (ISTE, London, 2007).

[40] O. Masson, R. Guinebretière, and A. Dauger, Reflection Debye-Scherrer powder diffraction with flat plate sample using CPS 120 INEL: D-spacing accuracy and Rietveld Refinement, J. Appl. Crystallogr. **29**, 540 (1996).

[41] Y. S. Touloukian, R. K. Kirby, R. E. Taylor, and T. Y. R. Lee, in *Thermophysical Properties of Matter* (Plenum, New York, 1977), Vol. 13, pp. 173–193.

[42] E. Kisi, *Zirconia Engineering Ceramics. Old Challenges - New Ideas* (Trans Tech, Zürich, 1998).

[43] H. Vazquez-Leal, R. Castaneda-Sheissa, U. Filobello-Nino, A. Sarmiento-Ryes, and J. Sanchez-Orea, High accurate simple approximation of normal distribution integral, Math. Problems Ing. **2012**, 124029 (2012).

[44] S. M. Lang, Axial thermal expansion of tetragonal $ZrO_2$ between 1150°C and 1700°C, J. Am. Ceram. Soc. **47**, 641 (1964).

[45] R. N. Patil and E. C. Subbarao, Axial thermal expansion of $ZrO_2$ and $HfO_2$ in the range room temperature to 1400°C, J. Appl. Crystallogr. **2**, 281 (1969).

[46] N. Igawa and Y. Ishii, Crystal structure of metastable tetragonal zirconia up to 1473 K, J. Am. Ceram. Soc. **84**, 1169 (2001).

[47] J. A. Krogstad, Y. Gao, J. Bai, J. Wang, D. M. Lipkin, and C. G. Levi, In situ diffraction study of the high-temperature decomposition of t'-zirconia, J. Am. Ceram. Soc. **98**, 247 (2015).

[48] J. D. Eshelby, The determination of the elastic field on an ellipsoidal inclusion and related problems, Proc. R. Soc. London, Ser. A **241**, 376 (1957).

[49] A. H. Heuer and M. Ruhle, and D. B. Marshall, On the thermoelastic martensitic transformation in tetragonal zirconia, J. Am. Ceram. Soc. **73**, 1084 (1990).

[50] R. C. Albers, R. Ahluwalia, T. Lookman, and A. Saxena, Modeling solid-solid phase transformations: From single crystal to polycrystal behavior, Comput. Appl. Math. **23**, 345 (2004).

[51] S. T. Reeve, K. G. Vishnu, and A. Strachan, Uncharacteristic second order martensitic transformation in metals via epitaxial stress fields, J. Appl. Phys. **127**, 045107 (2020).